Evolution of the Shape of the Raindrop Size Distribution in Simulated Shallow Cumulus

ANN KRISTIN NAUMANN

Max Planck Institute for Meteorology, Hamburg, Germany

AXEL SEIFERT

Hans-Ertel Centre for Weather Research, Deutscher Wetterdienst, Hamburg, Germany

(Manuscript received 2 September 2015, in final form 8 March 2016)

ABSTRACT

In this paper, the evolution of the raindrop size distribution (RSD) is investigated for two isolated shallow cumulus clouds that are modeled with large-eddy simulations. For a two-moment bulk rain microphysics scheme that assumes the RSD to follow a gamma distribution, it is shown that the evolution of the rainwater content of an individual shallow cumulus cloud—in particular, its subcloud-layer rainwater amount and its surface precipitation rate—is highly sensitive to the choice of the shape parameter of the gamma distribution.

To further investigate the shape of the RSD, a Lagrangian drop model is used to represent warm rain microphysics without a priori assumptions on the RSD. It is found that the shape parameter is highly variable in space and time and that existing closure equations, which are established from idealized studies of more heavily precipitating cases, are not appropriate for shallow cumulus. Although a relation of the shape parameter to the mean raindrop diameter is also found for individual shallow cumulus clouds, this relation differs already for the two clouds considered. It is therefore doubtful whether a two-moment scheme with a diagnostic parameterization of the shape parameter (i.e., a local closure in space and time) can be sufficient, especially when being applied across different cloud regimes. A three-moment bulk rain microphysics scheme is able to capture the general development of the relation of the shape parameter to the mean raindrop diameter for the two simulated clouds but misses some relevant features.

1. Introduction

Knowledge about the shape of the raindrop size distribution (RSD) is decisive for parameterizing bulk rain microphysics in atmospheric modeling as well as for deducing rain rates from observed radar reflectivity. The RSD is the spectral particle density $n(D)$, which is a function of equivalent diameter D and defined such that $n(D)dD$ is the number of particles per unit volume in the size range $[D, D + dD]$. In many applications, the RSD is assumed to follow the form of a gamma distribution

$$n(D) = N_0 D^{\mu} e^{-\lambda D}, \tag{1}$$

which has three free parameters: N_0 is referred to as the intercept, μ is the shape, and λ is the slope parameter (Ulbrich 1983; Kogan et al. 2009).

Warm bulk microphysics schemes usually distinguish between two hydrometeor classes: cloud water and rainwater (Kessler 1969; Beheng 1994). These two classes are separated in terms of a drop radius or mass, and both size distributions are often assumed to follow the form of a gamma distribution, which gives a bimodal distribution for the composite drop size distribution. Autoconversion and accretion as well as self-collection describe the conversion rates from one class to another and within one class, respectively [see Beheng (2010) for a recent review of bulk conversion rates]. In this study, we will focus on the rainwater class.

In three-moment bulk rain microphysics schemes, all three parameters of the gamma distribution are determined from the prognostic moments (Milbrandt and Yau 2005; Milbrandt and McTaggart-Cowan 2010). Although those schemes are potentially more accurate than single- or two-moment schemes, they also have to make simplifications in some microphysical processes (e.g., breakup and to a lesser extent evaporation) and

Corresponding author address: Ann Kristin Naumann, Max Planck Institute for Meteorology, Bundesstrasse 53, 20146 Hamburg, Germany.
E-mail: ann-kristin.naumann@mpimet.mpg.de

DOI: 10.1175/JAS-D-15-0263.1

how these processes modify the higher moments of the RSD. Also, reconstructing a gamma distribution from three moments—as opposed to reconstruction from one or two moments—may not necessarily be an advantage if the actual RSD deviates from a gamma distribution. Three-moment schemes are computationally more expensive than one- or two-moment schemes because of the additional prognostic variable.[1] So far, three-moment schemes are rarely used in large-scale models.

Single- and two-moment bulk rain microphysics schemes are widespread in atmospheric modeling [e.g., Kessler 1969; Beheng 1994; Walko et al. 1995; Feingold et al. 1998; Khairoutdinov and Kogan 2000; Seifert and Beheng 2001; Morrison et al. 2005; see Khain et al. (2015) for an extensive review]. In two-moment schemes, usually N_0 and λ are determined from the prognostic moments and μ, which is related to the width of the distribution, is fixed to a constant or diagnosed—for example, as a function of the mean raindrop diameter (Milbrandt and Yau 2005; Seifert 2008). In this study, we analyze the sensitivity of a two-moment bulk rain microphysics scheme to the choice of μ and investigate the evolution of μ in the course of a cloud's (rainwater) life cycle using the Lagrangian drop model from Naumann and Seifert (2015).

Especially in single-moment schemes (e.g., Kessler 1969), μ is often set to zero, which simplifies the gamma distribution to an inverse exponential distribution and has been suggested from measurements for raindrop diameters larger than 1.5 mm (Marshall and Palmer 1948). Because Marshall and Palmer (1948) were only able to measure such large diameters and also had to average over relatively long periods of time, this classical result should not be viewed as evidence for using $\mu = 0$ for all raindrop sizes and instantaneous distributions. Similar limitations arise for the equilibrium RSD (e.g., Hu and Srivastava 1995; McFarquhar 2004; Seifert et al. 2005; Barthes and Mallet 2013) because, especially for low rain rates, the RSD is often far from equilibrium (Barthes and Mallet 2013).

Reducing the number of independent parameters for the gamma distribution from three to two is not only of interest for parameterizing rain microphysics but is also necessary in the field of radar meteorology. For the latter, typically two independent remote measurements are obtained (e.g., reflectivity and attenuation) for a dual-wavelength radar or reflectivity at horizontal and vertical polarization for a polarimetric radar. To retrieve the RSD, which is again assumed to be well represented by the gamma distribution, a constraining relation is required. Analyzing disdrometer measurements, relations expressing μ as a function of λ have been proposed (e.g., Zhang et al. 2001, 2003; Brandes et al. 2003; Moisseev and Chandrasekar 2007; Munchak and Tokay 2008). Unfortunately, the applicability of those relations for parameterizing microphysical processes is limited for two reasons: First, the relation is found to be regionally and seasonally variable (Munchak and Tokay 2008) and it is not clear what is causing this variation. Second, all measurements are taken at the surface and are therefore not necessarily valid for the whole atmospheric column.

Concerning the second point, Geoffroy et al. (2014) analyzed in situ aircraft observations from two particle measurement devices in shallow cumulus. They find that μ is variable over orders of magnitude when related to the height or to different rain properties, such as the mean raindrop diameter. This broad range might be better understood if such data were analyzed for single rain events that are related to particular clouds and their life cycle rather than for a whole field of clouds. The high spatial and temporal resolution that would be required for such an in-depth analysis is difficult, if not impossible, to obtain from field measurements. Therefore, we will use high-resolution modeling to approach the issue in this study.

The decisive role of μ in determining microphysical process rates has been discussed in several idealized modeling studies. By considering sedimentation only (Milbrandt and Yau 2005; Wacker and Lüpkes 2009; Milbrandt and McTaggart-Cowan 2010) as well as taking into account all microphysical processes in a one-dimensional bin microphysics rainshaft model (Seifert 2008), different relations for μ as a function of the gridbox mean volume diameter $\overline{D}$ have been suggested. But those studies also show that the μ–$\overline{D}$ relation is variable, which suggests that an additional dependence is necessary to considerably reduce the present uncertainty in determining μ.

In this study, we investigate the variability of the RSD and the closure problem of a two-moment bulk scheme in a less idealized setup than recent modeling studies (e.g., Milbrandt and Yau 2005; Seifert 2008) have applied. The goal is to explain the variability of the μ–$\overline{D}$ relation by setting the evolution of μ in context to the life cycle of an individual cloud. In particular, we study a case of lightly precipitating shallow cumulus including the warm rain microphysical processes: sedimentation, evaporation, accretion, and self-collection. To achieve this, we use an LES model combined with a Lagrangian drop (LD) rain microphysics model (Naumann and Seifert 2015). The LD model simulates raindrop growth on a

[1] For UCLA-LES, we find a 6% increase in total run time for a shallow cumulus simulation using a three-moment scheme compared to a two-moment scheme.

particle-based level; that is, each LD follows its own trajectory and size evolution driven by the time-dependent, thermodynamical background fields of the Eulerian LES. Because the RSD in the LD model is not restricted to a prescribed distribution, the LD model is suited to study the evolution of the RSD and the shape parameter.

The rest of the paper is structured as follows. Section 2 shortly introduces the LES model, the LD model, and the shallow cumulus case setup. In section 3, we investigate the life cycle of two shallow cumulus clouds regarding their rainwater properties and microphysical processes for both the two-moment bulk scheme and the LD model. In section 4, we analyze the RSD and in particular the role of the shape parameter. Finally in section 5, we give some concluding remarks.

2. Model description and setup

The model setup used in this study is the same as for the control runs described in Naumann and Seifert (2015). In the following, we summarize the most important points.

a. Large-eddy simulation

We use the University of California, Los Angeles LES (UCLA-LES; Stevens et al. 2005; Stevens 2007) with a third-order Runge–Kutta scheme for time stepping. Prognostic equations are solved for the three components of the velocity, the total water mixing ratio, the liquid water potential temperature, the mass mixing ratio of rainwater, and the mass specific number of raindrops. Subgrid-scale fluxes are modeled with the Smagorinsky–Lilly model. Warm cloud and rain microphysical processes are parameterized by the two-moment bulk microphysics scheme of Seifert and Beheng (2001) with a diagnostic shape parameter (Seifert 2008) and a fixed cloud droplet density. We adjusted the density correction exponent in the terminal fall velocity to 0.35 to better fit the behavior of small raindrops.

For section 4 in this study, we have implemented a three-moment bulk rain microphysics scheme in UCLA-LES, which is described in the appendix.

b. Lagrangian drop model

The LD model simulates raindrop growth on a particle-based level after the initial formation of drizzle drops. Details of the LD model and its sensitivity to different model parameters can be found in Naumann and Seifert (2015). The methodology is closely related to the superdroplet method (Shima et al. 2009; Andrejczuk et al. 2010; Riechelmann et al. 2012) but focuses solely on the raindrop phase. Each LD represents a multiplicity of real raindrops with the same properties: that is, the same position, size, and velocity. The LD model does not replace the two-moment bulk rain microphysics scheme; instead it is one-way coupled with the Eulerian LES fields. To avoid inconsistencies, such a one-way coupling is only justified if the bulk rainwater field does not deviate substantially from the Lagrangian rainwater field. We will show later in section 3 that the two rainwater fields are indeed sufficiently similar.

The LDs are initialized proportional to the autoconversion rate of the two-moment bulk microphysics scheme to ensure that the same amount of rainwater is initialized in the bulk rain microphysics scheme and in the LD model. All relevant microphysical processes—accretion of bulk cloud water, self-collection among the LDs, and evaporation in unsaturated air—are included so that the mass of an LD evolves according to the environmental fields of the Eulerian LES. The momentum equation for each LD includes dynamical effects such as sedimentation and inertia and a contribution from the parameterized subgrid-scale fluid velocity. Naumann and Seifert (2015) show that the uncertainty of the LD model is much smaller than the uncertainty caused by the choice of the shape parameter in a two-moment bulk rain microphysics scheme.

c. Case setup

We use two variants of a case study of shallow cumulus over the ocean [Rain in Cumulus over the Ocean (RICO); Rauber et al. 2007] described by van Zanten et al. (2011) and Stevens and Seifert (2008), respectively. Both simulations apply a grid spacing of 25 m in all spatial directions. The domain size is $3.2 \times 3.2\,\mathrm{km}^2$ in the horizontal and 3.2 and 4.0 km in the vertical. Such a small domain has the advantage that there is basically a single cloud in the whole domain at one time. This allows us to analyze the time evolution of an individual cloud with relatively small computational effort and without the need to apply a complex cloud-tracking algorithm.

For each case study, we analyze the life cycle of one cloud and in the following, we refer to them as cloud A and cloud B. Both clouds considered in this study can be seen as random samples from a typical trade wind cumulus clouds ensemble. The life cycles of both clouds are simulated with the LES including the LD model. Each simulation lasts 1.5 h and output of the LD properties is written with a temporal resolution of 15 s.

3. Cloud life cycle

Snapshots of the rainwater content and the precipitation flux show similar spatial structures for the LD model and the two-moment bulk rain microphysics scheme (Fig. 1). Good agreement is also found for the

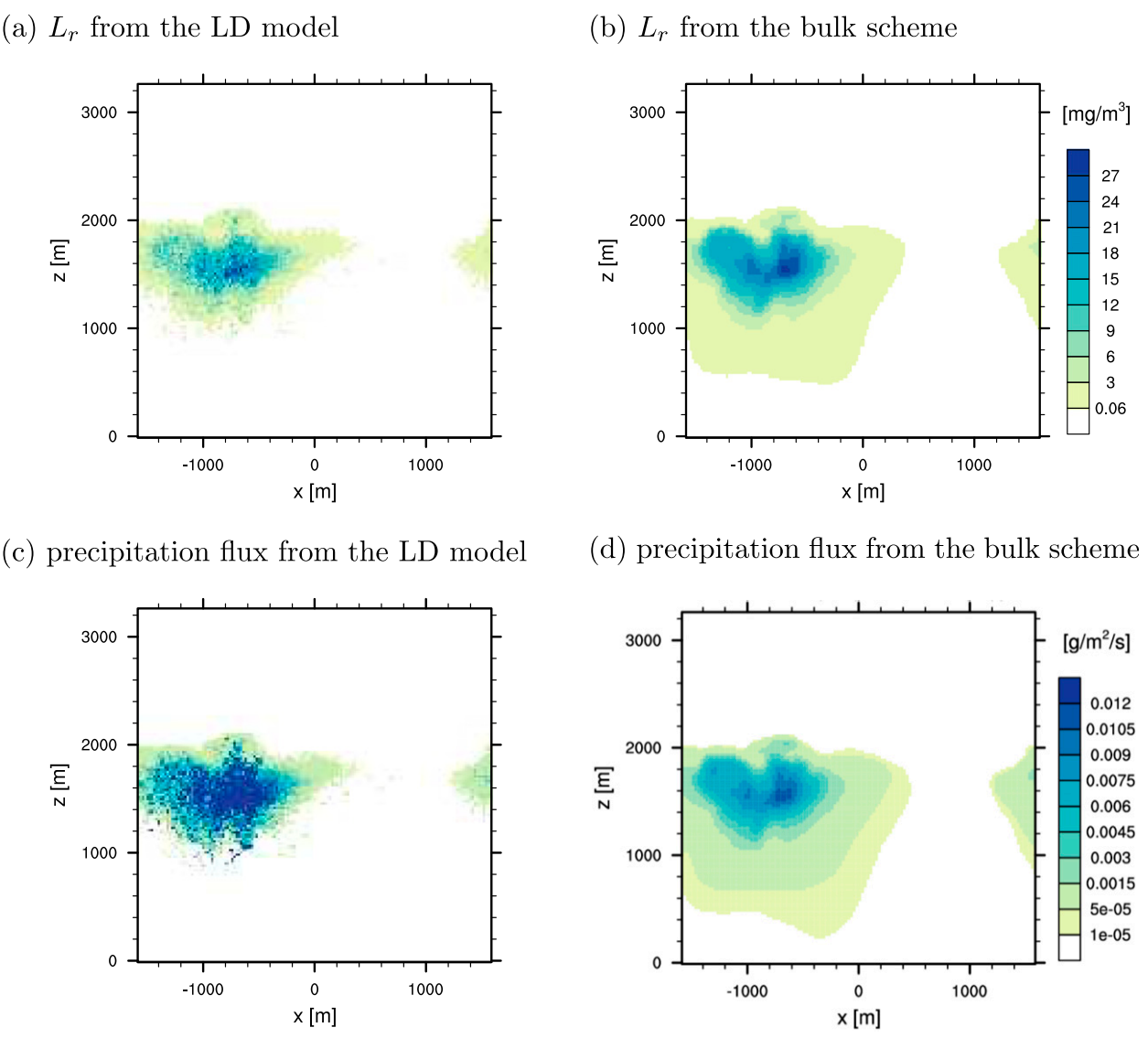

FIG. 1. Snapshot at $t = 30$ min averaged in the y direction for the rainwater content and the precipitation flux for cloud A.

temporal evolution of the profiles of the rainwater content and the raindrop number density (see discussion of Figs. 4 and 5 below). In the model, feedbacks to the dynamics are only considered from the two-moment scheme, and the LD model is run one-way coupled without any effect on the thermodynamic fields (see section 2b). Such a decoupling is justified in this case because the good agreement in rainwater properties in the two-moment scheme and the LD model suggests that the effect of the difference in the dynamics on the RSD is small.

A more critical examination of Fig. 1 does reveal some minor differences between the LD model and the two-moment scheme. Compared to the LD model, the two-moment scheme is too diffusive, which becomes apparent in a broad area of low rainwater content and low precipitation flux surrounding the area with high values. In addition, the maximum rainwater content and the maximum precipitation flux have lower values in the two-moment scheme than in the LD model. To better understand this difference, we first analyze the (rainwater) life cycle of cloud A and cloud B and then investigate the differences between the rainwater properties from the LD model and the two-moment scheme in more detail.

The temporal evolution of cloud A and cloud B with respect to their rainwater amount and the microphysical rates is quite different (Fig. 2). While for cloud A the peak overall rainwater amount is twice as high as for cloud B, the period of time that considerable rainwater amount is present in the domain is shorter for cloud A

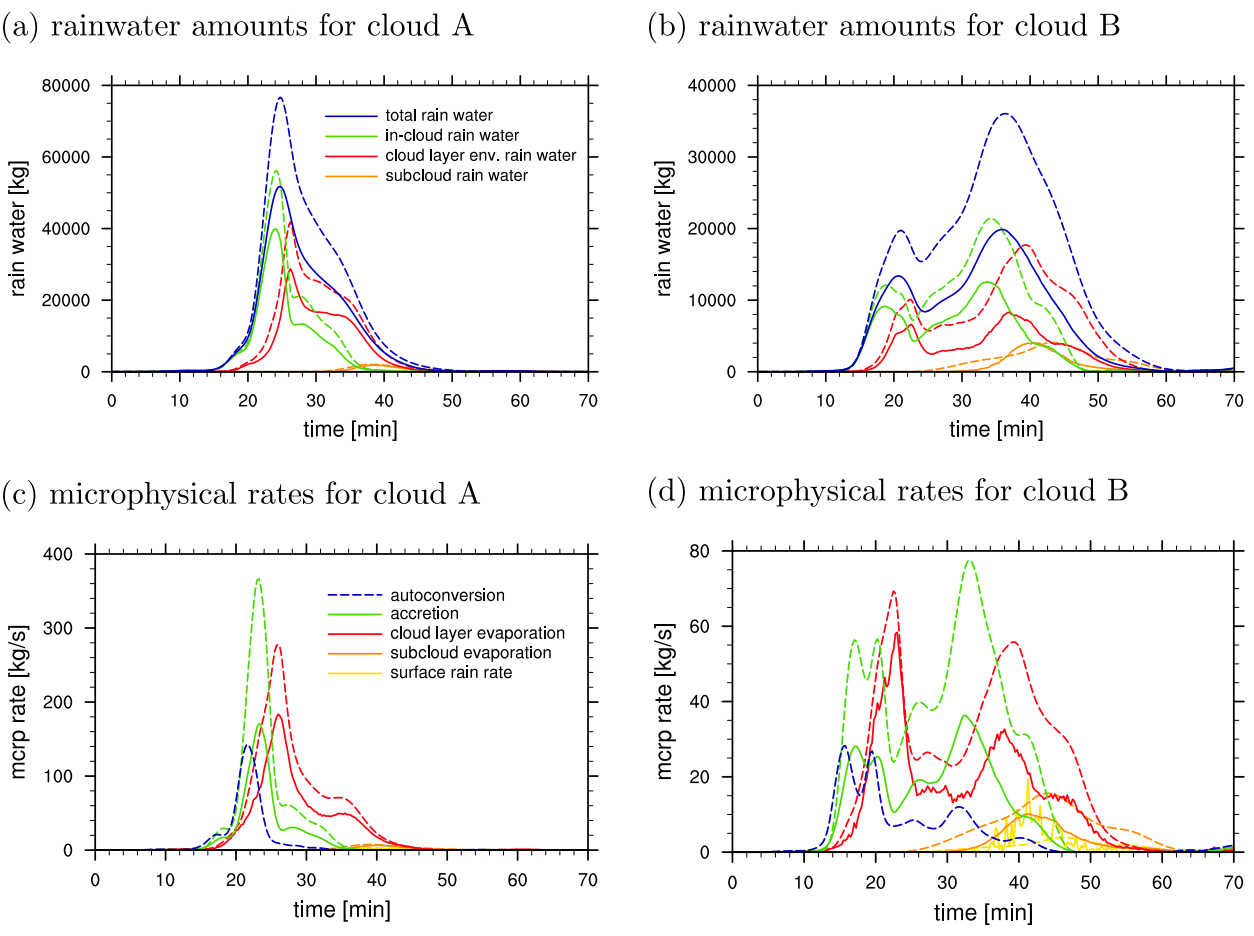

FIG. 2. Life cycles of two isolated shallow cumulus clouds in terms of their rainwater properties. Shown are rainwater amounts and microphysical rates in the whole domain. Solid lines represent results from the LD model and dashed lines represent results from the two-moment bulk scheme. Note the different scales on the *y* axes.

than for cloud B by about 10 min. This is a result of the different dynamics and consequently different microphysical rates in both simulations.

For cloud A, we find one main updraft at around 20 min where the cloud water content is high near cloud top and where therefore a high autoconversion rate transforms cloud water to rainwater in the two-moment scheme (Fig. 3a). Soon after this relatively short initiation period with a high autoconversion rate, the accretion rate increases and starts to dominate rainwater gain (Fig. 2c). Because rainwater gain through accretion occurs inside the cloud and rainwater is lost through evaporation outside the cloud, we describe the life cycle of the cloud in terms of its in-cloud rainwater, its cloud-layer environmental rainwater (i.e., rainwater in the cloud layer but outside the cloud, which is defined by the presence of bulk cloud water), and its subcloud-layer rainwater (Fig. 2a). Initially, most of the rainwater is found inside the cloud but in the subsequent evolution this changes in short order. The rainwater found in the cloud-layer environment increases and reduces the in-cloud rainwater. At this point, evaporation of rainwater starts to decrease the overall rainwater amount drastically (Fig. 2c).

Only a very small fraction of the overall rainwater amount in the domain is found in the subcloud layer (Fig. 2a). This implies that almost all rainwater leaves the cloud through its lateral boundaries rather than through cloud base. The maximum subcloud-layer rainwater is found approximately 15 min after the maximum in total rainwater. This delay might be explained by two processes, which are closely related. First, newly initiated raindrops need time to grow through accretion and self-collection to become so large that they develop a considerable fall velocity to be able to fall below cloud base. Second, the autoconversion rate is maximum near cloud top between 2000 and 2500 m and it takes the raindrops time to cover the distance, whether through cloudy or environmental air, until cloud-base level (around 600 m).

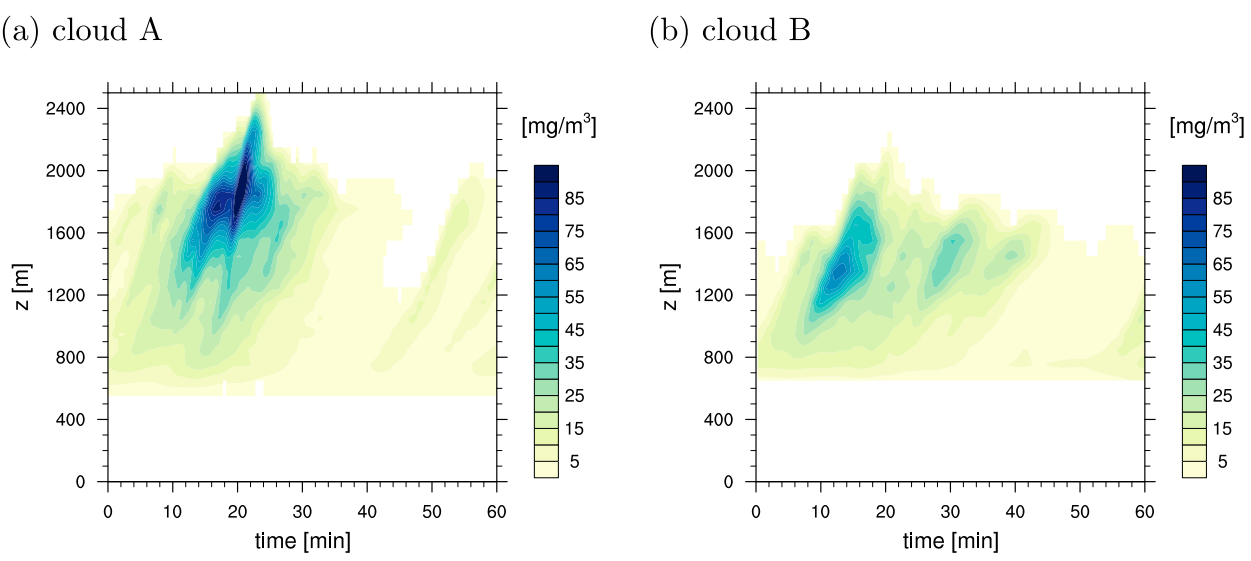

FIG. 3. Temporal evolution of the profiles of the domain-averaged cloud water content.

In contrast to the simple life cycle of cloud A, which rather closely aligns with our understanding of an idealized precipitating shallow cumulus cloud, the picture is more complex for cloud B. Here, several smaller cloud water maxima in the time evolution of cloud water are found (Fig. 3b). Accordingly, several autoconversion and subsequent accretion and evaporation events take place and have cumulative effects (Figs. 2b,d). For example, the autoconversion rate has five maxima or pulses during the lifetime of cloud B. Such a pulsating growth is a common feature for shallow cumulus clouds (Rauber et al. 2007; Heus et al. 2009). Analyzing LES runs of different shallow cumulus cases, Heus et al. (2009) find on average four pulses per cloud. This indicates that cloud B might be more representative for a typical shallow cumulus cloud than cloud A.

Compared to cloud A, the occurrence of rainwater in the domain is considerably prolonged for cloud B and rainwater builds up so that rainwater amount only maximizes after 25 min (Fig. 2b). The total rainwater amount is smaller for cloud B than for cloud A owing to weaker updrafts and overall lower autoconversion and accretion rates. In contrast to cloud A, the raindrops in cloud B are able to grow over a longer period of time, and the amount of rainwater in the subcloud layer relative to the total rainwater amount and also the surface precipitation rate are higher (Fig. 2d).

Comparing the rainwater properties of the LD model and the two-moment scheme, the onset of precipitation in the subcloud layer is more sudden in the LD model (Figs. 4 and 5). This is especially evident in terms of the mean raindrop volume diameter:

$$\overline{D} = \left(\frac{6}{\pi\rho_w}\frac{L_r}{N_r}\right)^{1/3}, \tag{2}$$

where L_r is the rainwater content, N_r is the raindrop number density, and ρ_w is the density of water. In the LD model, the largest raindrops reach the subcloud layer first; that is, $\overline{D}$ is initially large and then decreases with time. In the two-moment scheme, the onset of precipitation in the subcloud layer occurs substantially earlier and overall smoother compared to the LD model. This early onset of surface precipitation is the result of excessive gravitational sorting, which is a known issue in two-moment bulk rain microphysics schemes and will be discussed further in section 4a.

In the two-moment scheme, L_r initially increases faster than N_r and therefore $\overline{D}$ initially increases near the surface. Because of the overall earlier onset in the two-moment scheme, the maximum value of $\overline{D}$ is reached earlier in the two-moment scheme than in the LD model. Also, the maximum value of $\overline{D}$ is larger for the LD model than for the two-moment scheme. In the subsequent period after the maximum value of $\overline{D}$, L_r decreases in the subcloud layer more rapidly for the LD model than for the two-moment scheme. Accordingly, $\overline{D}$ also decreases faster for the LD model than for the two-moment scheme.

Note that, early in the simulation, rainwater properties of the preceding cloud can be found in the two-moment bulk scheme but not in the LD model because the LDs have not been initialized for the preceding cloud. For the analyzed cloud, the absence of the preceding rainwater has no effect on the results of the LD model.

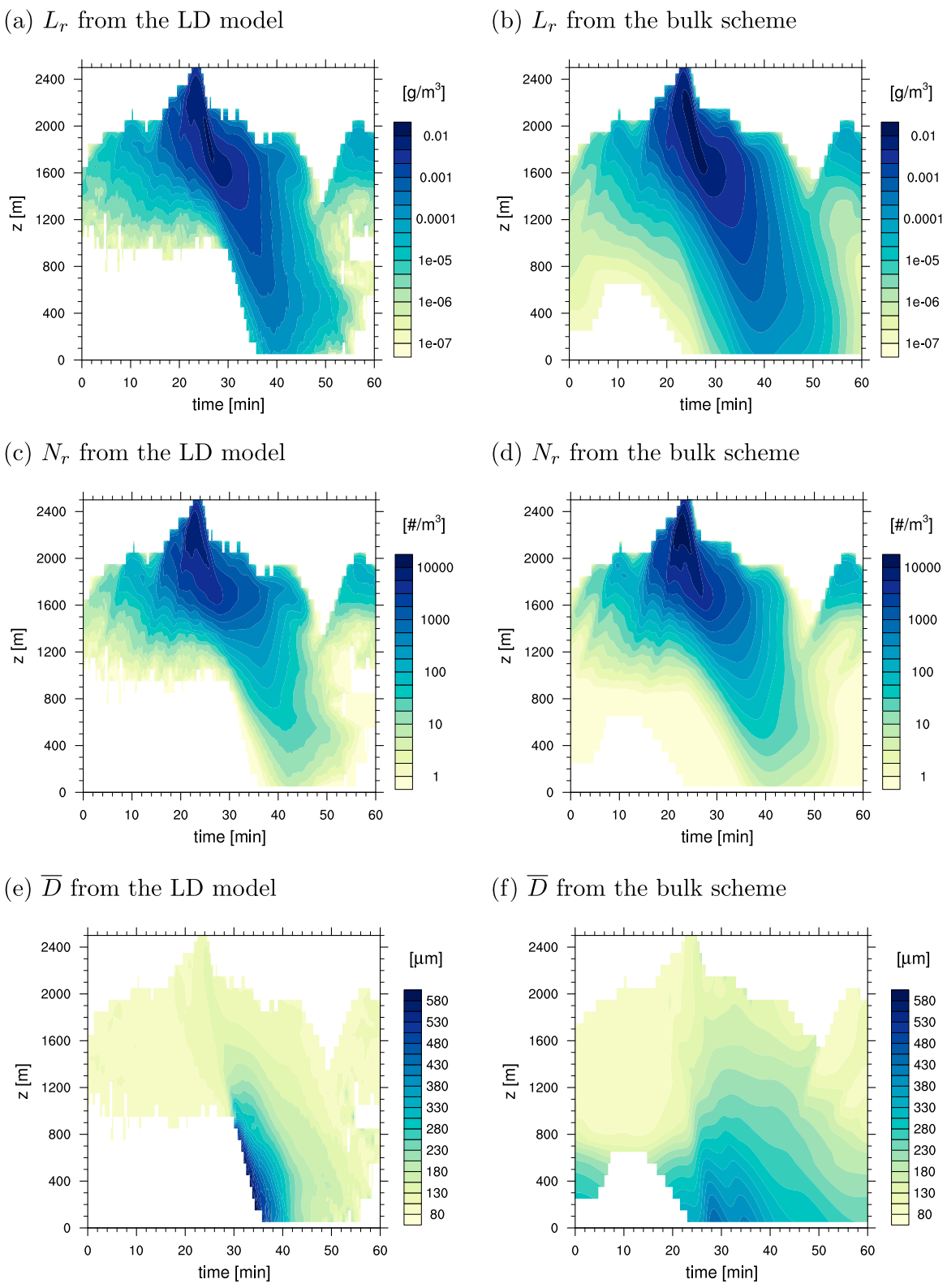

FIG. 4. Temporal evolution of the profiles of domain-averaged properties for cloud A. (a)–(d) Note the logarithmic scale. (b),(d),(f) For the two-moment bulk scheme, areas with $L_r < 10^{-7}\,\mathrm{g\,m^{-3}}$ are blanked out.

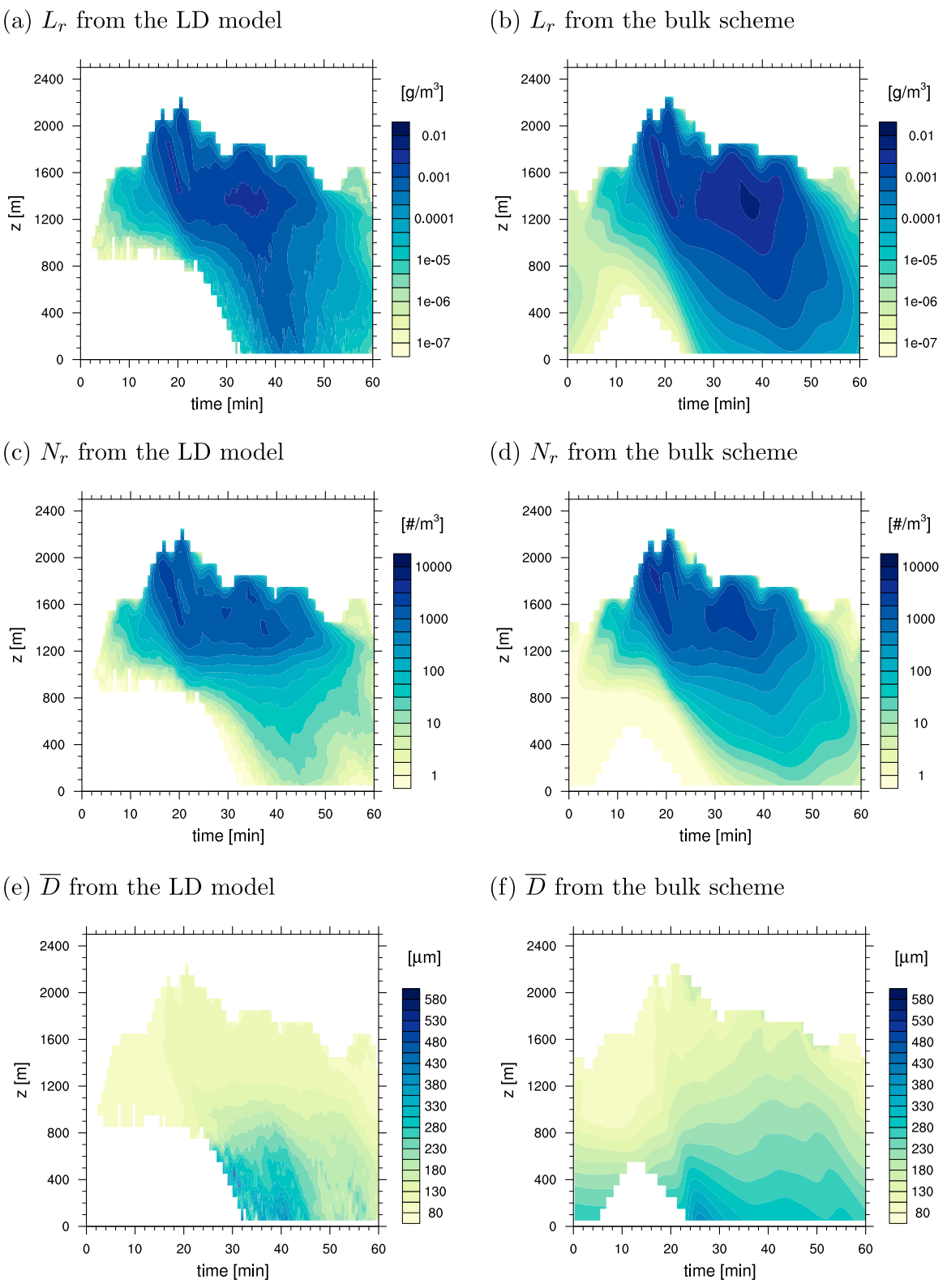

FIG. 5. As in Fig. 4, but for cloud B.

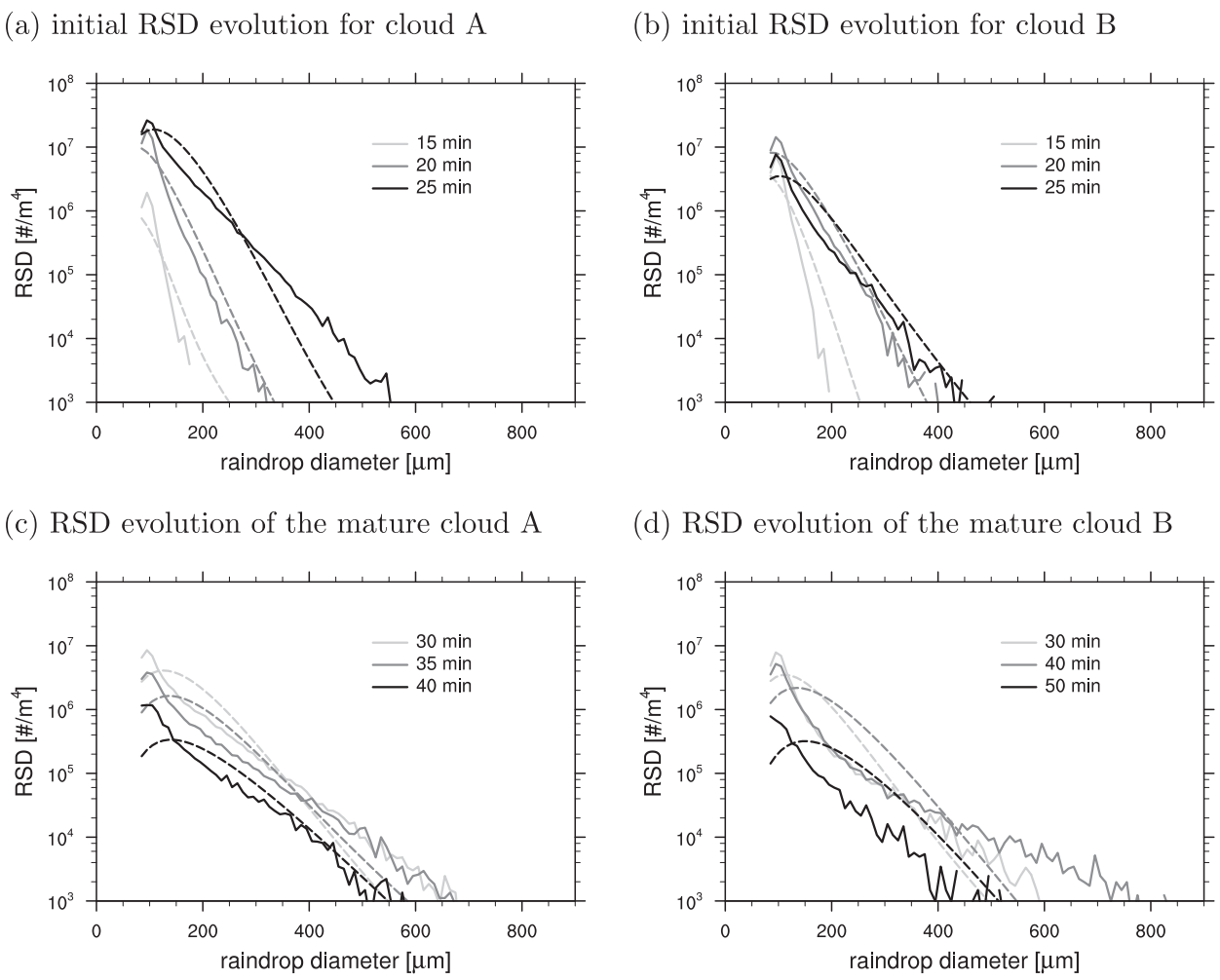

FIG. 6. Temporal evolution of the mean RSD for the whole domain. Solid lines represent results from the LD model and dashed lines represent results from the two-moment bulk scheme.

Differences between the LD model and the two-moment scheme are also found for the microphysical rates (Figs. 2c,d). Although by design of the model the autoconversion rate generates bulk rainwater and LD rainwater in same amounts, the accretion rate is lower for the LDs than for the two-moment scheme for both clouds over their whole life cycle. As a result, the total rainwater and the evaporation rate are also lower for the LD model.

The cause for these differences can be found in the RSDs (Fig. 6). For both clouds, when the first rainwater forms, the RSD determined from the LDs is slightly narrower than the one diagnosed and employed in the two-moment scheme (Figs. 6a,b). Therefore, the initial production of rainwater mass through accretion is less effective for the LDs and thus influences the subsequent rainwater evolution. Nevertheless, RSD broadening is stronger for the LDs and the largest raindrops with a diameter larger than 500 μm form more frequently than in the two-moment scheme (Figs. 6c,d).

Therefore, though the total rainwater amount of the two-moment scheme is higher, the subcloud-layer rainwater amount and also the surface precipitation rate, which are both sensitive to the largest raindrops, are higher for the LDs (Fig. 2). This effect can also be seen in the snapshots of the horizontally averaged, vertical cross sections (Fig. 1). Though the maximum absolute value of the rainwater content is larger for the two-moment scheme, the precipitation flux is larger for the LD model because it is dominated by the largest raindrops, which fall fastest. The difference between the LD model and the two-moment scheme in the distribution of the largest raindrops (i.e., in the tail of the RSDs) can mostly be attributed to the in-cloud RSDs (Fig. 7).

For all diameter sizes, the in-cloud RSD shows a decrease in the number density of raindrops with increasing

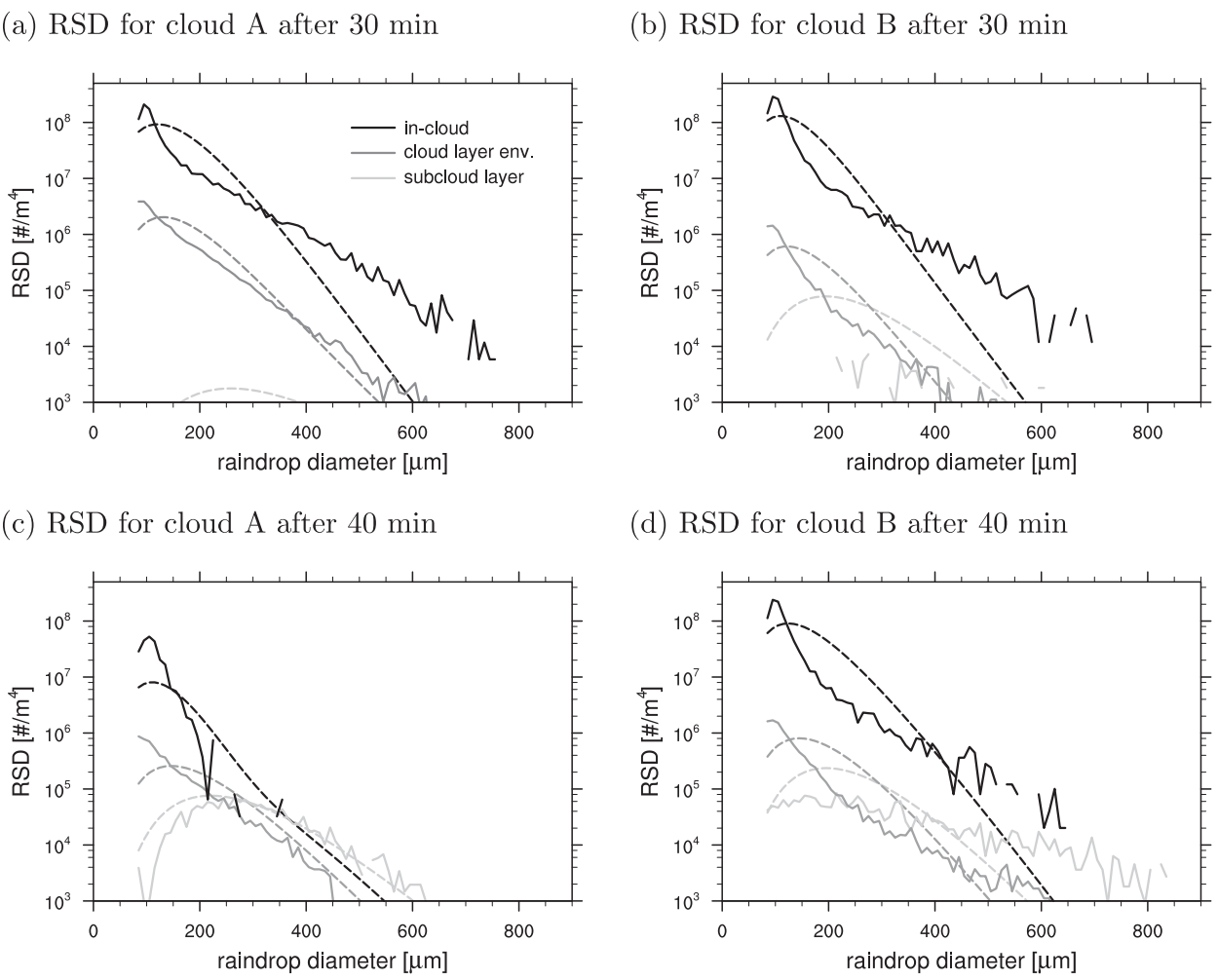

FIG. 7. RSD within the cloud, in the environmental cloud layer, and in the subcloud layer. Solid lines represent results from the LD model and dashed lines represent results from the two-moment bulk scheme.

diameter. In contrast, for the subcloud layer, gravitational sorting is strong and the number density of raindrops increases for increasing raindrop diameters less than 200 μm. For the subcloud layer of cloud A, the RSD of the LDs is in surprisingly good agreement with the RSD in the two-moment scheme (Fig. 7c). For the subcloud layer of cloud B, the RSD of the LDs is broader than the RSD in the two-moment scheme, which does not allow for such a flat RSD (Fig. 7d).

4. The RSD's shape parameter

Microphysical process rates depend on the shape of the RSD. Therefore, two-moment bulk rain microphysics schemes that represent the RSD by a gamma distribution [Eq. (1)] are known to be sensitive to the choice of the shape parameter of the gamma distribution μ. To investigate the role of μ, we adopt two approaches. First, we discuss the effect of μ on the rain properties in the two-moment bulk rain microphysics scheme and compare them to the rain properties from the LD model and from a three-moment bulk rain microphysics scheme. Second, we use the LD statistics and the three-moment scheme to discuss how μ evolves over the course of the simulation and what that implies for the parameterizability of μ in a two-moment scheme.

a. *Sensitivity of the two-moment bulk scheme to the RSD's shape parameter*

Besides the diagnostic relation of Seifert (2008), which has been used for the simulations discussed in section 3, another diagnostic relation has been suggested by Milbrandt and Yau (2005). In addition to those two variants, we conduct two more simulations where μ is fixed to either 1 or 10. Considering the uncertain knowledge of the value of the shape parameter, also such a

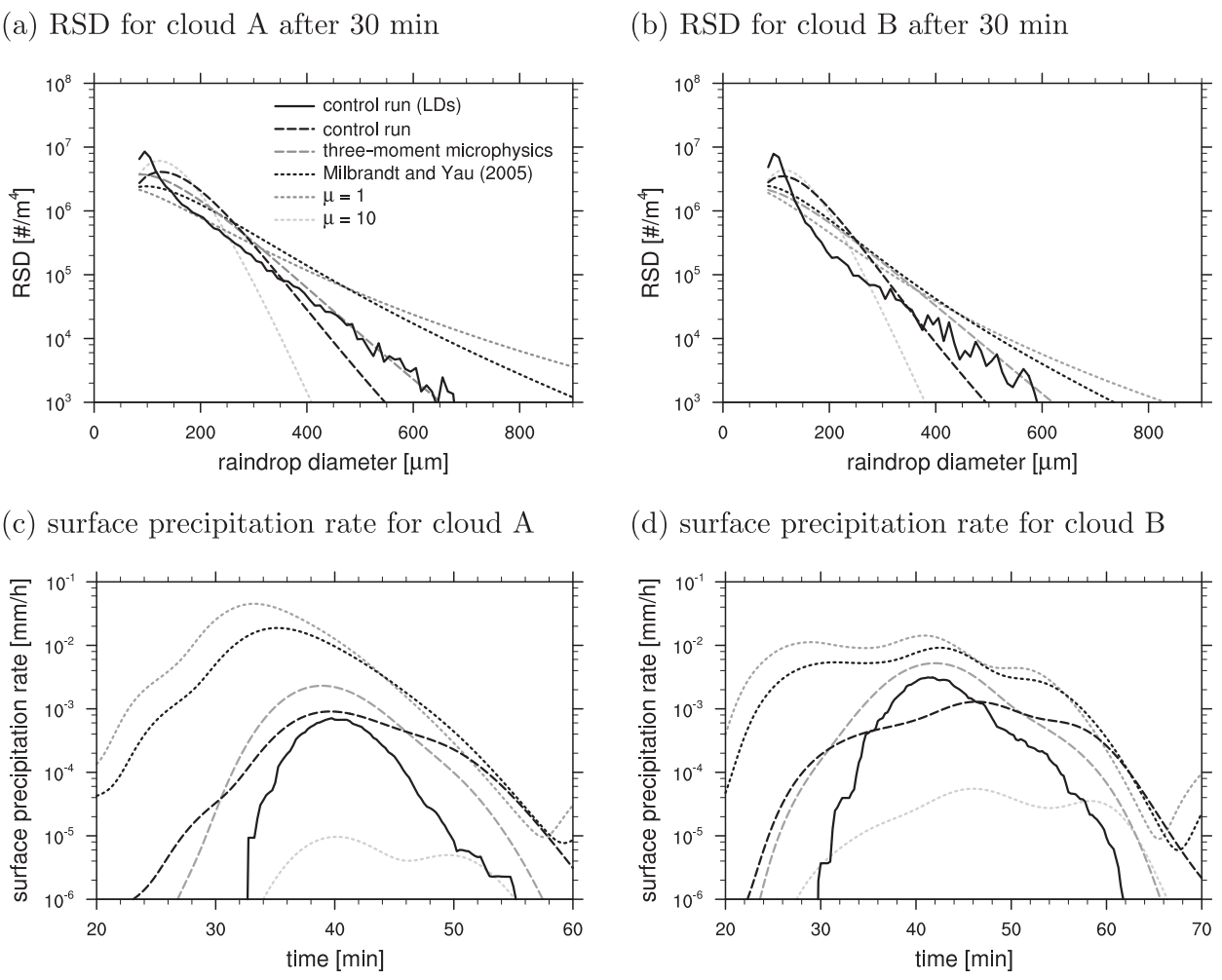

FIG. 8. Domain-average RSD and surface precipitation rate using different values for the shape parameter μ in the two-moment bulk scheme. Solid lines represent results from the LD model and dashed lines represent results from the two- and three-moment bulk schemes.

constant value of 1 or 10 is a plausible choice (Stevens and Seifert 2008). Because in our simulations $\overline{D}$ is always smaller than 700 μm, the diagnostic relation from Seifert (2008) effectively corresponds to a constant value of $\mu = 7$.

Furthermore, we conduct one simulation with a three-moment bulk rain microphysics scheme. In the three-moment scheme, the rainwater reflectivity is added as a third prognostic variable in addition to the raindrop number density and the rainwater content. In this way, all three parameters of the gamma distribution—N_0, λ, and μ—are determined by the prognostic variables. A description of the three-moment bulk rain microphysics scheme and the relation of μ to the prognostic variables is given in the appendix.

As the value of μ gets smaller, the RSD becomes broader and more rain reaches the surface. Compared to the RSD from the LD model, two-moment bulk rain microphysics schemes with large μ (i.e., narrow distributions) perform best during the very first stage of rain formation in the cloud (Figs. 6 and 8). In contrast, the two-moment schemes with smaller μ seem more reasonable in a later stage. If μ is chosen too small, the amplitude of the surface precipitation rate is considerably overestimated by the two-moment scheme compared to the LD approach (Fig. 8). The RSDs from the three-moment scheme and the LD model after 30 min of simulation are in very good agreement, especially for the tail of the distribution. The three-moment scheme overestimates the surface precipitation rate compared to the LD model during the whole simulation but the difference is less than for the two-moment schemes with small μ.

Surprisingly, the differences in RSD and surface precipitation rate are larger for the simpler cloud A than for

the more complex cloud B. We speculate that this is related to a more explosive evolution of cloud A, which might be less well represented by a bulk scheme, or to the multipulse evolution of cloud B, which might give opportunity to deplete remaining condensate in the next pulse.

The relative differences in surface rain discussed above may appear very large in part because the overall surface precipitation is small for shallow cumulus and because we are looking at an individual cloud instead of averaging over a larger area with a cloud ensemble. Related to this, an intercomparison study, analyzing the RICO case with several different LES models using different microphysical parameterizations, showed that many features of the cloud layer were in good agreement among the models, but considerable differences were encountered in the cloud microphysical structure and the surface precipitation rate (van Zanten et al. 2011). This indicates that the RICO case might be rather sensitive to microphysical choices especially when using small domain sizes as it is usually done. In addition, for short integration times, rain rates are less constrained by the vertical structure and the imposed forcing. Thus, we expect differences (e.g., in surface precipitation) not to be as pronounced for other, heavier precipitating cases or when using larger domains and averaging over longer time periods.

Regardless of the choice of μ, we find an earlier onset of surface precipitation for the two-moment scheme than for the LD model (Figs. 8c,d). This is in agreement with other studies that attribute the early onset of surface precipitation for two-moment schemes to an overestimation of gravitational sorting in the sedimentation process, which is due to the differences in sedimentation speed for the two moments considered (Wacker and Seifert 2001; Milbrandt and Yau 2005; Morrison and Grabowski 2007). This bias is a characteristic of the two-moment equations and cannot be eliminated by a simple retuning of some parameters, like the shape parameter. As shown by Wacker and Seifert (2001), bulk schemes eliminate the most important variable for size sorting (the size) and by this a nonlinear equation emerges from the previously linear sedimentation equation. In one- and two-moment bulk schemes, the RSD does not become narrower when the largest raindrops fall out because the shape is prescribed either as a fixed value or by some diagnostic relation. This leads to an artificial spectral transfer; that is, the large raindrops that fall out are immediately created again. Excessive size sorting can to some extent be fixed by controlling the ratio of the sedimentation velocities as suggested by Milbrandt and McTaggart-Cowan (2010) as well as Mansell (2010), but such ad hoc modifications can lead to inconsistencies in the physical assumptions of the scheme.

b. *Evolution of the RSD's shape parameter in the LD model and in the three-moment bulk scheme*

For the LDs, the RSD is not bound to a gamma distribution but can evolve freely. Assuming that the LD RSD is well represented by a gamma distribution [Eq. (1)], the distribution's parameters can be estimated from the first three moments of the RSD. To have a sufficient sample for the RSD, we estimate the distribution's parameter only if there are more than 50 LDs within a vertical layer of 100 m for one output time step. We find that μ is widely varying with time and height, but some more general behavior can be deduced from the two simulations of lightly precipitating shallow cumulus (Fig. 9):

1) Large values for μ (i.e., narrow RSDs) are found near cloud top where raindrops are created by autoconversion at similar sizes and where the mean volume diameter is close to the initial raindrop diameter (Figs. 4e and 5e). However, one should be cautious with a physical interpretation of the large values of μ at the initial appearance of rainwater in the cloud layer because the smallest raindrop sizes are subject to assumptions made in the LD model. First, the initial size of a LD is set artificially by assuming an initial size distribution as described in Naumann and Seifert (2015) and second, the RSD is truncated below D = 80 μm [see Handwerker and Straub (2011) and Johnson et al. (2011) for a discussion of the latter issue]. Both model choices limit the reliability of the estimate of μ for the initial RSD.
2) In the cloud layer, μ decreases with decreasing height and progressing cloud lifetime. The RSD broadens with time as a result of self-collection and because different trajectories allow for different growth histories of the raindrops. As most of the LDs originate near cloud top, RSDs in lower cloud layers are typically older and therefore broader. The mixing of particles with trajectories of different origin and history is an important mechanism for the observed, rapid broadening of drop size distributions in small cumulus clouds. Here, we simulate only the final growth stage from small to large raindrops and the broadening of the RSD. The growth stage from cloud droplets to raindrops and the broadening of the cloud droplet size distribution has been the focus of several earlier studies (Cooper 1989; Lasher-Trapp et al. 2005; Devenish et al. 2012; Cooper et al. 2013; Grabowski and Wang 2013).

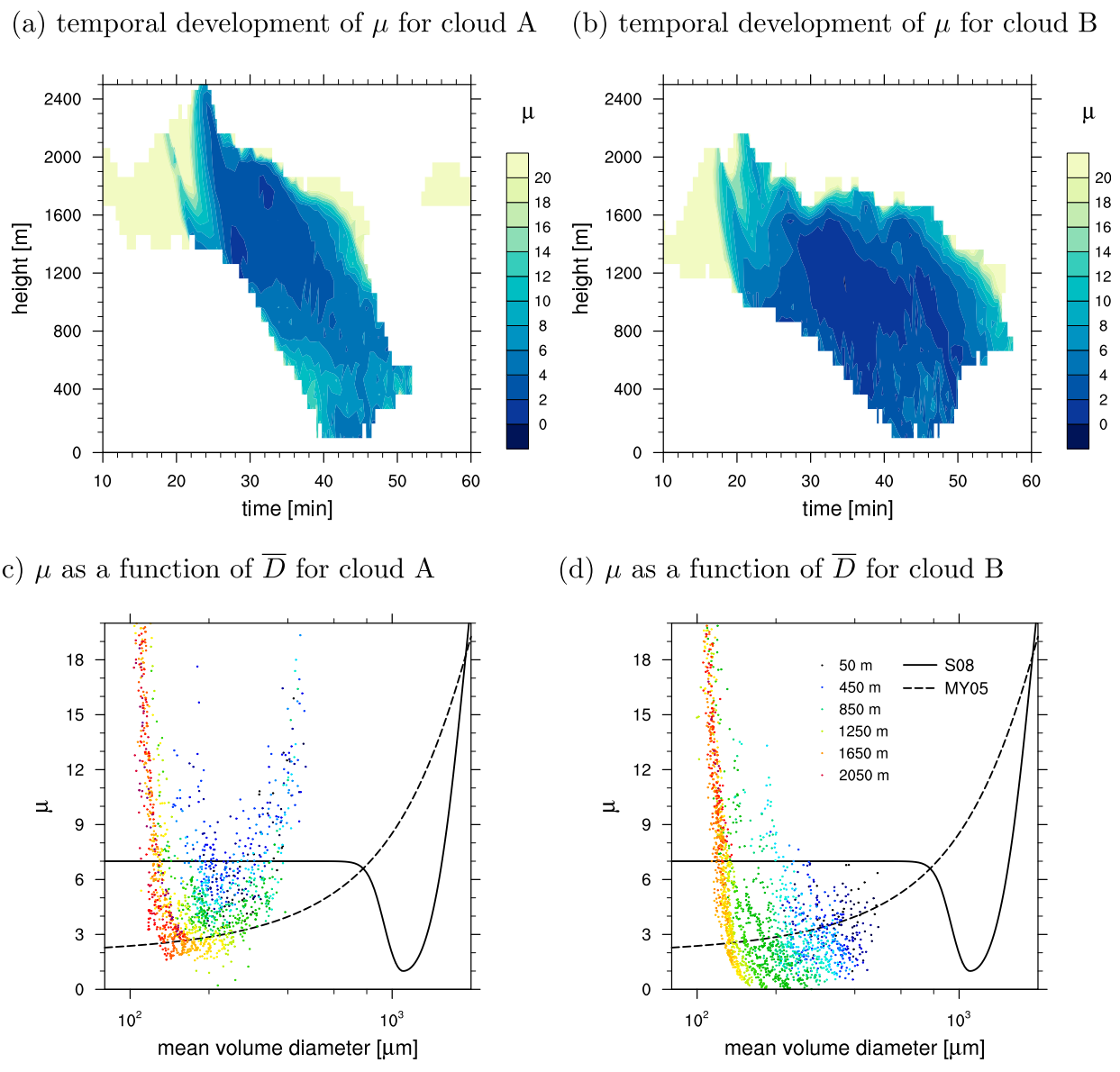

FIG. 9. Evolution of the shape parameter in the LD model: (a),(b) μ as a function of height and time and (c),(d) μ as a function of the mean raindrop diameter colored by height. Additionally in (c) and (d), the closure equations from Seifert (2008, S08) and Milbrandt and Yau (2005, MY05) are plotted.

3) For cloud A, three stages can be identified in the subcloud layer that have also been described in more idealized studies (e.g., by Seifert 2005). First, large values for μ are found when the first raindrops reach the subcloud layer. Because of gravitational sorting the largest raindrops reach the subcloud layer first, which gives a narrow distribution with a large mean diameter. With time, μ decreases in the subcloud layer because smaller raindrops eventually follow the first large ones. In this second stage, the RSD becomes broader while the mean raindrop diameter decreases. Finally, μ increases again while the mean diameter still decreases. At this stage the largest raindrops have already reached the ground while some smaller ones remain in the subcloud layer. Together with the broadening of the RSD in the cloud layer (point 2 in this list), these three stages in the subcloud layer show up as a V shape in the μ–$\overline{D}$ relation (Fig. 9c).
4) For cloud B, which—unlike cloud A—is characterized by several pulses of autoconversion events (see section 3), the second and third stages can be identified in a similar manner whereas the first stage of extensive gravitational sorting is not found. In the

second stage, the RSD becomes broader for cloud B than for cloud A and μ decreases below values of 1. The lack of extensive gravitational sorting and the stronger broadening of the RSD might be explained by the more complex evolution of cloud B, which allows for a larger variability in LD trajectories. For cloud B, raindrops need to be supported for a relatively long time in the upper part of the cloud layer to grow to the largest sizes because the rainwater content is lower than for cloud A. Then moderately large raindrops fall out first (when they are not supported by an updraft anymore) while the largest raindrops (that ''luckily'' had been supported longer and were therefore able to grow most) fall out later but are able to outpace the moderately large raindrops. Therefore, the early RSDs in the subcloud layer are already relatively broad.

Based on the described phenomenology and process understanding, and on earlier studies (e.g., Seifert 2005), we expect the V shape of the μ–$\overline{D}$ relation, which is found for cloud A, to be a robust feature for single-pulse clouds. For more complex clouds, like the multipulse cloud B, the V shape might not be a common feature. For cloud B, the right-hand-side branch, which is attributed to extensive gravitational sorting, is missing. In addition to the occurrence of gravitational sorting, also the position of the minimum in the μ–$\overline{D}$ relation seems to be case dependent, which makes a general parameterization of μ as a function of $\overline{D}$ difficult for individual clouds. The difficulty of a single μ–$\overline{D}$ relation to represent different individual clouds does not directly imply a systematic effect for an ensemble of clouds; that is, it does not exclude that an appropriate μ–$\overline{D}$ relation could be able to well represent the development of the average RSD of an ensemble of clouds.

In three-moment bulk rain microphysics schemes, μ is not prescribed as a function of D but is determined from the three prognostic variables and can therefore take into account the individual development of a particular cloud. In our simulation, the three-moment scheme is able to capture the different development of μ in cloud A and cloud B although there are some differences to the LD model (Fig. 10). The V shape of the μ–$\overline{D}$ relation for cloud A in the LD model is also found for the three-moment scheme but the right-hand-side branch is less pronounced; that is, the RSD in the subcloud layer is initially narrower in the LD model than in the three-moment scheme. Also, in the three-moment scheme the left-hand-side branch is generated only by the upper layers of the cloud and not by the subcloud layer; that is, the RSD remains broad in the subcloud layer in the three-moment scheme (Fig. 10c). We expect these differences to result, at least partly, from the simplifications used in the formulation of the microphysical processes and how they modify the reflectivity in the three-moment scheme.

5. Conclusions

In this study, we investigate the life cycle of shallow cumulus clouds regarding their rainwater properties with a focus on the evolution of the shape of the RSD. Two isolated shallow cumulus clouds are simulated with LES. The properties of the rainwater field of each cloud are studied, both with a commonly used two-moment warm rain bulk microphysics scheme and with an LD model.

In contrast to the evolution of the rainwater for cloud A, which is characterized by a single autoconversion event and subsequently evolving accretion and evaporation rates, the evolution of cloud B is more complex. Here, several overlapping autoconversion events result in a less distinct temporal separation of the autoconversion, accretion, and evaporation phase. This multipulse evolution of cloud B allows for a large variability of LD trajectories and hence a strong broadening of the RSD. For both clouds, the RSD in the LD model is initially narrower than what is assumed in the two-moment bulk scheme but broadens more in the course of time. Therefore, though the overall rainwater mass is less for the LD model than for the two-moment scheme, the subcloud-layer rainwater mass and the surface precipitation rate are in a similar range.

However, this is only true if the shape parameter μ of the RSD in the two-moment bulk scheme is diagnosed by the relation suggested by Seifert (2008), which we use for the control runs. Fixing μ to a lower constant value or using the diagnostic relation suggested by Milbrandt and Yau (2005) broadens the RSD and consequently has a quite drastic effect—for example, on the surface precipitation rate. Though this large effect may be partly due to the relatively low overall precipitation rate in shallow cumulus, it points to the important role of μ in the two-moment bulk rain microphysics scheme. Other uncertainties in the microphysical process rates—for example, the assumption that the gamma distribution well represents the RSD or the description of the collision and the coalescence efficiencies in the accretion and self-collection rates—also contribute to the uncertainty in simulated rainwater properties but are not discussed in this study.

Investigating the evolution of μ derived from the LD statistics, we find a robust broadening of the initial RSD, with μ rapidly decreasing to values less than 3. How broad the RSD becomes and whether it narrows again in

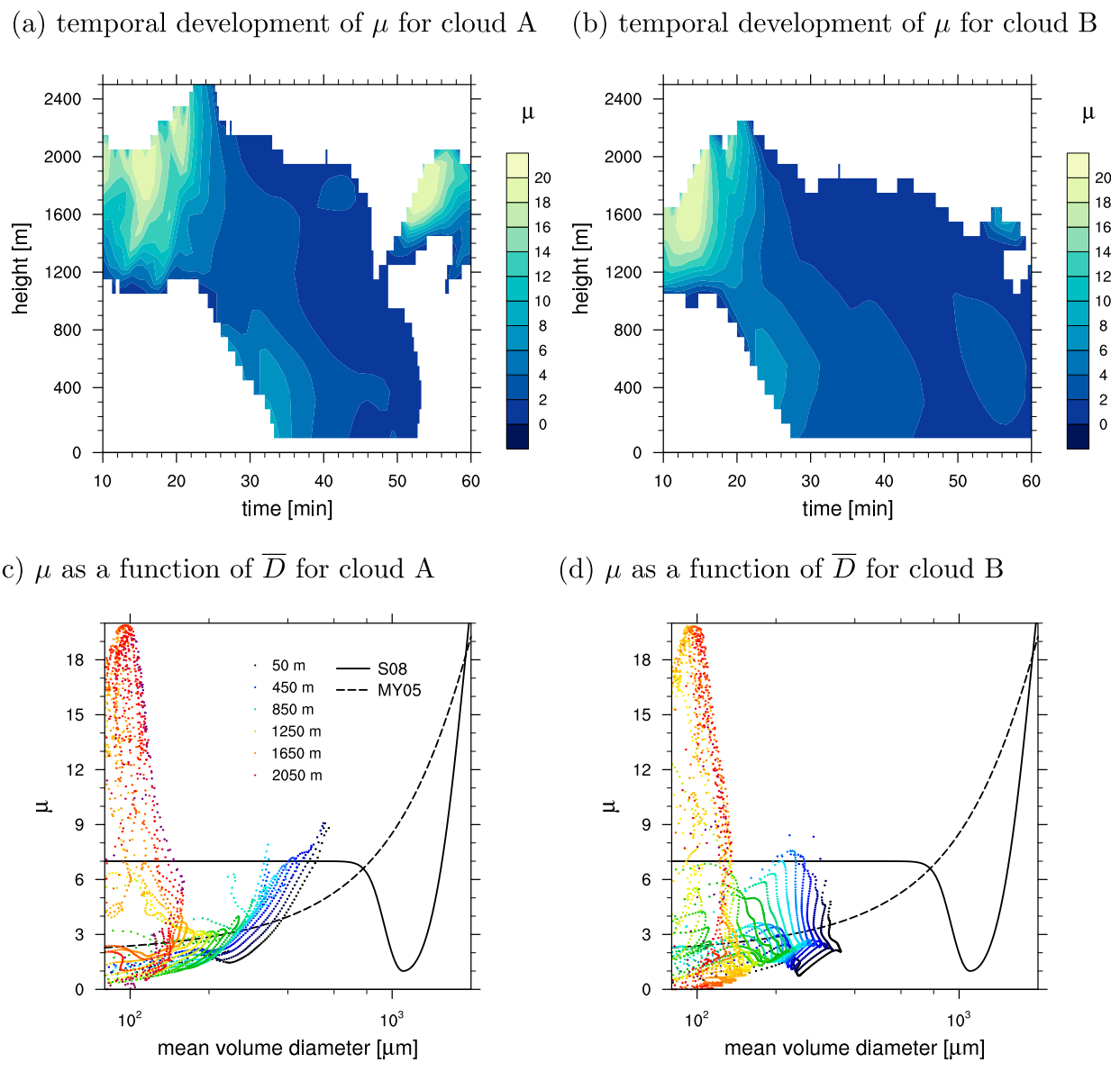

FIG. 10. As in Fig. 9, but with μ derived from the three-moment bulk rain microphysics.

the subcloud layer depends on the effectiveness of gravitational sorting. For the single-pulse cloud A, we find a V-shaped μ–$\overline{D}$ relation. The left-hand-side descending branch represents the initial broadening of the RSD, which is caused by the different trajectories and growth histories of the LDs. The right-hand-side ascending branch of the V shape represents a narrowing of the RSD in the subcloud layer due to extensive gravitational sorting and is not found for the multipulse cloud B.

This indicates that, for the simple, single-pulse cloud A, the results are in good agreement with idealized studies that described the V shape before (e.g., Seifert 2005). For more complex life cycles, the μ–$\overline{D}$ relation has to be modified. A V-shaped relation though shifted substantially toward larger mean diameters has also been found by Seifert (2008) for stronger rain events. In more heavily precipitating clouds, larger raindrops are more common owing to deeper cloud layers, higher rainwater contents, and more vigorous updrafts. Hence, gravitational sorting becomes dominant only at larger diameters and the μ–$\overline{D}$ relation shifts toward those larger diameters. Milbrandt and Yau (2005) also focused on stronger precipitation events just taking into account sedimentation and, consequently, only found an ascending branch toward large diameters. Because

shallow cumulus precipitation is restricted to relatively small raindrops, both published μ–$\overline{D}$ relations fail to represent the detailed evolution of μ for individual shallow cumulus clouds. A three-moment bulk rain microphysics scheme is able to capture the general development of the μ–$\overline{D}$ relation for cloud A and cloud B but misses some features such as a narrowing of the RSD in the subcloud layer toward the end of the rainwater life cycle.

The results of this study suggest that parameterizing μ solely as a function of $\overline{D}$ in two-moment bulk rain microphysics schemes is not appropriate for individual clouds if different cloud regimes and different complexities of cloud life cycles are considered. The position of the minimum in the μ–$\overline{D}$ relation, the occurrence of the ascending branch, and presumably also the slopes of the branches might depend on other variables such as on overall precipitation, updraft speed, or cloud depth. Rather than the mean raindrop diameter, a classification according to the stage of the RSD's evolution could also be useful. Therefore, a nonlocal closure in time—that is, a parameterization that has explicit knowledge about the current state of the cloud relative to its overall life cycle—might ultimately be needed in two-moment bulk rain microphysics schemes if the error that arises from the μ–$\overline{D}$ closure is judged to be too large. Three-moment schemes, computationally more expensive than two-moment schemes, overcome the need for such a closure and provide a promising alternative to two-moment schemes.

Acknowledgments. We thank Bjorn Stevens, Vivek Sant, Jason Milbrandt, and two anonymous reviewers for their valuable comments, which helped to improve the manuscript. Primary data and scripts used in the analysis and other supplementary information that may be useful in reproducing the author's work are archived by the Max Planck Institute for Meteorology and can be obtained by contacting publications@mpimet.mpg.de. This research was carried out as part of the Hans-Ertel Centre for Weather Research. This research network of universities, research institutes, and Deutscher Wetterdienst is funded by the BMVI (Federal Ministry of Transport and Digital Infrastructure).

APPENDIX

Description of a Three-Moment Bulk Rain Microphysics Scheme

Here we provide the equations of the three-moment bulk warm rain scheme. These equations are a consistent extension of the Seifert and Beheng (2001) parameterization and, consequently, they differ in some details from other existing three-moment schemes like Milbrandt and Yau (2005). A more detailed discussion of the suggested three-moment scheme will be given elsewhere (A. Seifert and A. K. Naumann 2016, unpublished manuscript).

As prognostic variables, we use the first three mass moments of the RSD $M_r^{(k)}$, with $k \in [0, 1, 2]$:

$$M_r^{(k)} = \int_0^\infty f(x) x^k \, dx = \left(\frac{\pi \rho_w}{6}\right)^k \int_0^\infty n(D) D^{3k} \, dD, \tag{A1}$$

where x is the raindrop mass and $f(x)$ is the spectral particle density as a function of the raindrop mass. For the first three moments of the gamma distribution [Eq. (1)], we find explicitly

$$N_r = M_r^{(0)} = \frac{N_0 \Gamma(\mu + 1)}{\lambda^{\mu+1}}, \tag{A2}$$

$$L_r = M_r^{(1)} = \left(\frac{\pi \rho_w}{6}\right) \frac{N_0 \Gamma(\mu + 4)}{\lambda^{\mu+4}}, \quad \text{and} \tag{A3}$$

$$Z_r = M_r^{(2)} = \left(\frac{\pi \rho_w}{6}\right)^2 \frac{N_0 \Gamma(\mu + 7)}{\lambda^{\mu+7}}, \tag{A4}$$

where N_r is raindrop number density, L_r is rainwater content, and Z_r is rainwater reflectivity. The three moments determine the three distribution parameters N_0, λ, and μ. To calculate μ, we evaluate the dimensionless parameter $N_r Z_r / L_r^2$, which is only a function of μ:

$$G(\mu) = \frac{(\mu + 4)(\mu + 5)(\mu + 6)}{(\mu + 1)(\mu + 2)(\mu + 3)} = \frac{N_r Z_r}{L_r^2}. \tag{A5}$$

We solve for the root of this equation using Cardano's formula (e.g., Abramowitz and Stegun 1972, p. 17).

For the terminal fall velocity of rain drops $v_r(D)$, we apply an Atlas-type relation with $v_r(D) = \alpha_r - \beta_r \exp(-\gamma_r D)$, with α_r, β_r, and γ_r as given by Stevens and Seifert (2008). For the sedimentation velocities of all mass moments including reflectivity, we find

$$\overline{v}_{r,k} = \left(\frac{\rho_0}{\rho_a}\right)^{0.35} \left[\alpha_r - \beta_r \left(1 + \frac{\gamma_r}{\lambda}\right)^{-(3k+\mu+1)}\right], \tag{A6}$$

which includes a correction for the density dependence of the sedimentation velocity with ρ_0 being the reference air density and ρ_a being the actual air density. Note that $\overline{v}_{r,k} \geq \overline{v}_{r,k-1}$; that is, higher moments fall faster leading to gravitational sorting.

For autoconversion, we apply the concept of a separation of the drop size distribution in two categories by a threshold mass, $x_* = 2.6 \times 10^{-10}$ kg, which corresponds

to a threshold drop diameter of $D_* = 80\,\mu$m. We assume further that the raindrop embryos created by autoconversion follow a uniform distribution in the size range $[x_*, 2x_*]$. The same assumptions are made in the LD model of Naumann and Seifert (2015). This yields

$$\left.\frac{\partial N_r}{\partial t}\right|_{au} = \frac{2}{3}\frac{1}{x_*}\left.\frac{\partial L_r}{\partial t}\right|_{au} \quad \text{and} \tag{A7}$$

$$\left.\frac{\partial Z_r}{\partial t}\right|_{au} = \frac{14}{9}x_*\left.\frac{\partial L_r}{\partial t}\right|_{au}. \tag{A8}$$

In this case the mass rate for autoconversion is sufficient to specify the corresponding rates of all other moments.

For accretion, we use the definition of that process given by Beheng's formulation (Beheng and Doms 1986; Doms and Beheng 1986; Beheng 2010):

$$\left.\frac{\partial M_r^{(k)}}{\partial t}\right|_{ac} = \int_0^{x_*}\int_{x_*}^{\infty} f(x')f(x'')K(x',x'')[(x'+x'')^k - x'^k - x''^k]\,dx'\,dx'' \tag{A9}$$

and apply the linear part of Long's kernel:

$$K(x',x'') = k_r(x'+x''), \tag{A10}$$

which is valid in the accretion regime. With some simplifications, we find the accretion rate

$$\left.\frac{\partial Z_r}{\partial t}\right|_{ac} = 2k_r L_c Z_r, \tag{A11}$$

where L_c is the cloud water content. For consistency with the mass accretion rate of the Seifert and Beheng (2001) scheme, we include the similarity function $\Phi_{ac}(\tau)$ and the density correction in the accretion rate for reflectivity

$$\left.\frac{\partial Z_r}{\partial t}\right|_{ac} = 2k_r L_c Z_r \Phi_{ac}(\tau)\left(\frac{\rho_0}{\rho_a}\right)^{0.35}. \tag{A12}$$

For self-collection, we can also apply Long's kernel and find

$$\left.\frac{\partial Z_r}{\partial t}\right|_{sc} = 2k_r Z_r N_r, \tag{A13}$$

but this equation proves to be insufficient. Therefore, we apply the variance approximation of Seifert et al. (2014) to parameterize the self-collection rate. For the number density and reflectivity, we find

$$\left.\frac{\partial N_r}{\partial t}\right|_{sc} = \frac{\pi}{4}N_r^2\overline{\Delta v}_0\overline{E}_{\mathrm{coal},n}\lambda^{-2}(\mu+1)^2\left(1+\frac{\mu+2}{\mu+1}\right) \tag{A14}$$

and

$$\left.\frac{\partial Z_r}{\partial t}\right|_{sc} = \frac{\pi}{2}Z_r N_r\overline{\Delta v}_1\overline{E}_{\mathrm{coal},z}\lambda^{-2}\frac{(\mu+1)(\mu+2)(\mu+3)(\mu+4)}{(\mu+5)(\mu+6)}\left(1+\frac{\mu+5}{\mu+4}\right), \tag{A15}$$

with the bulk velocity difference given by

$$\overline{\Delta v}_n^2 = 2\beta_r^2\left[\left(\frac{\lambda}{\lambda+2\gamma_r}\right)^{\nu_n} - \left(\frac{\lambda}{\lambda+\gamma_r}\right)^{2\nu_n}\right], \tag{A16}$$

with $\nu_n = \mu + 3 + 3n$ and γ_r is the coefficient of the Atlas-type terminal fall velocity relation. For the bulk coalescence efficiency, we use

$$\overline{E}_{\mathrm{coal},z}(\overline{D}) = \max[0.53(1-\alpha_{\mathrm{coal}}\overline{D}),\,0.0] \tag{A17}$$

based on the empirical parameterizations of Beard and Ochs (1995) and Low and List (1982) and with $\alpha_{\mathrm{coal}} = 0.69\times10^3\,\mathrm{m}^{-3}$. The latter value is based on a numerical integration of the collection integral (A9) for a gamma distribution and has only a weak dependency on μ, which can be neglected. Note that we apply this coalescence efficiency only to the equation for Z_r while we set $\overline{E}_{\mathrm{coal},n} = 1$ because the self-collection of the number density is dominated by small droplets.

The bulk evaporation equations for L_r and Z_r are given by

$$\left.\frac{\partial L_r}{\partial t}\right|_{eva} = \int_{D_*}^{\infty}\left.\frac{\partial x}{\partial t}\right|_{eva} n(D)\,dD \quad \text{and} \tag{A18}$$

$$\left.\frac{\partial Z_r}{\partial t}\right|_{eva} = \int_{D_*}^{\infty}\left.\frac{\partial x}{\partial t}\right|_{eva} n(D)x(D)\,dD, \tag{A19}$$

with the evaporation rate of an individual drop being linear in drop diameter D. If we make the simplification that ventilation effects affect reflectivity in the same way as mass, then we find

$$\left.\frac{\partial Z_r}{\partial t}\right|_{eva} = \overline{x}\frac{(\mu+4)}{(\mu+1)}\left.\frac{\partial L_r}{\partial t}\right|_{eva}. \tag{A20}$$

Neglecting the fact that ventilation effects are different for mass and reflectivity leads to a slight overestimation of reflectivity because ventilation would act more strongly on reflectivity than on rainwater content. At least for precipitating shallow cumulus and stratocumulus, this can probably be ignored. For the number rate due to evaporation, we follow Seifert (2008) and apply

$$\left.\frac{\partial N_r}{\partial t}\right|_{\text{eva}} = \gamma_{\text{eva}} \frac{1}{\bar{x}} \left.\frac{\partial L_r}{\partial t}\right|_{\text{eva}} \tag{A21}$$

but with the simpler relation $\gamma_{\text{eva}} = \exp(-0.1\mu)$. This takes into account that a narrow RSD leads to a reduced change in number density due to evaporation.

REFERENCES

Abramowitz, M., and I. A. Stegun, 1972: *Handbook of Mathematical Functions*. 9th ed. Dover, 1046 pp.

Andrejczuk, M., W. W. Grabowski, J. Reisner, and A. Gadian, 2010: Cloud-aerosol interactions for boundary layer stratocumulus in the Lagrangian Cloud Model. *J. Geophys. Res.*, **115**, D22214, doi:10.1029/2010JD014248.

Barthes, L., and C. Mallet, 2013: Vertical evolution of raindrop size distribution: Impact on the shape of the DSD. *Atmos. Res.*, **119**, 13–22, doi:10.1016/j.atmosres.2011.07.011.

Beard, K. V., and H. T. Ochs, 1995: Collisions between small precipitation drops. Part II: Formulas for coalescence, temporary coalescence, and satellites. *J. Atmos. Sci.*, **52**, 3977–3996, doi:10.1175/1520-0469(1995)052<3977:CBSPDP>2.0.CO;2.

Beheng, K. D., 1994: A parameterization of warm cloud microphysical conversion processes. *Atmos. Res.*, **33**, 193–206, doi:10.1016/0169-8095(94)90020-5.

——, 2010: The evolution of raindrop spectra: A review of basic microphysical essentials. *Rainfall: State of the Science*, *Geophys. Monogr.*, Vol. 191, Amer. Geophys. Union, 29–48.

——, and G. Doms, 1986: A general formulation of collection rates of cloud and raindrops using the kinetic equation and comparison with parameterizations. *Contrib. Atmos. Phys.*, **59**, 66–84.

Brandes, E. A., G. Zhang, and J. Vivekanandan, 2003: An evaluation of a drop distribution-based polarimetric radar rainfall estimator. *J. Appl. Meteor.*, **42**, 652–660, doi:10.1175/1520-0450(2003)042<0652:AEOADD>2.0.CO;2.

Cooper, W. A., 1989: Effects of variable droplet growth histories on droplet size distributions. Part I: Theory. *J. Atmos. Sci.*, **46**, 1301–1311, doi:10.1175/1520-0469(1989)046<1301:EOVDGH>2.0.CO;2.

——, S. G. Lasher-Trapp, and A. M. Blyth, 2013: The influence of entrainment and mixing on the initial formation of rain in a warm cumulus cloud. *J. Atmos. Sci.*, **70**, 1727–1743, doi:10.1175/JAS-D-12-0128.1.

Devenish, B., and Coauthors, 2012: Droplet growth in warm turbulent clouds. *Quart. J. Roy. Meteor. Soc.*, **138**, 1401–1429, doi:10.1002/qj.1897.

Doms, G., and K. D. Beheng, 1986: Mathematical formulation of self-collection, autoconversion and accretion rates of cloud and raindrops. *Meteor. Rundsch.*, **39**, 98–102.

Feingold, G., R. L. Walko, B. Stevens, and W. R. Cotton, 1998: Simulations of marine stratocumulus using a new microphysical parameterization scheme. *Atmos. Res.*, **47–48**, 505–528, doi:10.1016/S0169-8095(98)00058-1.

Geoffroy, O., A. P. Siebesma, and F. Burnet, 2014: Characteristics of the raindrop distribution in RICO shallow cumulus. *Atmos. Chem. Phys.*, **14**, 10 897–10 909, doi:10.5194/acp-14-10897-2014.

Grabowski, W. W., and L.-P. Wang, 2013: Growth of cloud droplets in a turbulent environment. *Annu. Rev. Fluid Mech.*, **45**, 293–324, doi:10.1146/annurev-fluid-011212-140750.

Handwerker, J., and W. Straub, 2011: Optimal determination of parameters for gamma-type drop size distributions based on moments. *J. Atmos. Oceanic Technol.*, **28**, 513–529, doi:10.1175/2010JTECHA1474.1.

Heus, T., H. J. J. Jonker, H. E. A. Van den Akker, E. J. Griffith, M. Koutek, and F. H. Post, 2009: A statistical approach to the life cycle analysis of cumulus clouds selected in a virtual reality environment. *J. Geophys. Res.*, **114**, D06208, doi:10.1029/2008JD010917.

Hu, Z., and R. C. Srivastava, 1995: Evolution of raindrop size distribution by coalescence, breakup, and evaporation: Theory and observations. *J. Atmos. Sci.*, **52**, 1761–1783, doi:10.1175/1520-0469(1995)052<1761:EORSDB>2.0.CO;2.

Johnson, R. W., D. V. Kliche, and P. L. Smith, 2011: Comparison of estimators for parameters of gamma distributions with left-truncated samples. *J. Appl. Meteor. Climatol.*, **50**, 296–310, doi:10.1175/2010JAMC2478.1.

Kessler, E., 1969: *On the Distribution and Continuity of Water Substance in Atmospheric Circulations*. *Meteor. Monogr.*, No. 32, Amer. Meteor. Soc., 84 pp.

Khain, A. P., and Coauthors, 2015: Representation of microphysical processes in cloud-resolving models: Spectral (bin) microphysics versus bulk parameterization. *Rev. Geophys.*, **53**, 247–322, doi:10.1002/2014RG000468.

Khairoutdinov, M., and Y. Kogan, 2000: A new cloud physics parameterization in a large-eddy simulation model of marine stratocumulus. *Mon. Wea. Rev.*, **128**, 229–243, doi:10.1175/1520-0493(2000)128<0229:ANCPPI>2.0.CO;2.

Kogan, Y. L., Z. N. Kogan, and D. B. Mechem, 2009: Fidelity of analytic drop size distributions in drizzling stratiform clouds based on large-eddy simulations. *J. Atmos. Sci.*, **66**, 2335–2348, doi:10.1175/2009JAS3028.1.

Lasher-Trapp, S., W. A. Cooper, and A. M. Blyth, 2005: Broadening of droplet size distribution from entrainment and mixing in a cumulus cloud. *Quart. J. Roy. Meteor. Soc.*, **131**, 195–220, doi:10.1256/qj.03.199.

Low, T. B., and R. List, 1982: Collision, coalescence and breakup of raindrops, Part I: Experimentally established coalescence efficiencies and fragment size distributions in breakup. *J. Atmos. Sci.*, **39**, 1591–1606, doi:10.1175/1520-0469(1982)039<1591:CCABOR>2.0.CO;2.

Mansell, E. R., 2010: On sedimentation and advection in multimoment bulk microphysics. *J. Atmos. Sci.*, **67**, 3084–3094, doi:10.1175/2010JAS3341.1.

Marshall, J. S., and W. M. K. Palmer, 1948: The distribution of raindrops with size. *J. Meteor.*, **5**, 165–166, doi:10.1175/1520-0469(1948)005<0165:TDORWS>2.0.CO;2.

McFarquhar, G. M., 2004: A new representation of collision-induced breakup of raindrops and its implications for the shapes of raindrop size distributions. *J. Atmos. Sci.*, **61**, 777–794, doi:10.1175/1520-0469(2004)061<0777:ANROCB>2.0.CO;2.

Milbrandt, J. A., and M. K. Yau, 2005: A multimoment bulk microphysics parameterization. Part I: Analysis of the role of the spectral shape parameter. *J. Atmos. Sci.*, **62**, 3051–3064, doi:10.1175/JAS3534.1.

——, and R. McTaggart-Cowan, 2010: Sedimentation-induced errors in bulk microphysics schemes. *J. Atmos. Sci.*, **67**, 3931–3948, doi:10.1175/2010JAS3541.1.

Moisseev, D. N., and V. Chandrasekar, 2007: Examination of the μ–Λ relation suggested for drop size distribution parameters. *J. Atmos. Oceanic Technol.*, **24**, 847–855, doi:10.1175/JTECH2010.1.

Morrison, H., and W. W. Grabowski, 2007: Comparison of bulk and bin warm-rain microphysics models using a kinematic framework. *J. Atmos. Sci.*, **64**, 2839–2861, doi:10.1175/JAS3980.

——, J. A. Curry, and V. I. Khvorostyanov, 2005: A new double-moment microphysics parameterization for application in cloud and climate models. Part I: Description. *J. Atmos. Sci.*, **62**, 1665–1677, doi:10.1175/JAS3446.1.

Munchak, S. J., and A. Tokay, 2008: Retrieval of raindrop size distribution from simulated dual-frequency radar measurements. *J. Appl. Meteor. Climatol.*, **47**, 223–241, doi:10.1175/2007JAMC1524.1.

Naumann, A. K., and A. Seifert, 2015: A Lagrangian drop model to study warm rain microphysical processes in shallow cumulus. *J. Adv. Model. Earth Syst.*, **7**, 1136–1154, doi:10.1002/2015MS000456.

Rauber, R. M., and Coauthors, 2007: Rain in shallow cumulus over the ocean: The RICO campaign. *Bull. Amer. Meteor. Soc.*, **88**, 1912–1924, doi:10.1175/BAMS-88-12-1912.

Riechelmann, T., Y. Noh, and S. Raasch, 2012: A new method for large-eddy simulations of clouds with Lagrangian droplets including the effects of turbulent collision. *New J. Phys.*, **14**, doi:10.1088/1367-2630/14/6/065008.

Seifert, A., 2005: A note on the shape–slope relation of the drop size distribution in convective rain. *J. Appl. Meteor.*, **44**, 1146–1151, doi:10.1175/JAM2254.1.

——, 2008: On the parameterization of evaporation of raindrops as simulated by a one-dimensional rainshaft model. *J. Atmos. Sci.*, **65**, 3608–3619, doi:10.1175/2008JAS2586.1.

——, and K. D. Beheng, 2001: A double-moment parameterization for simulating autoconversion, accretion and selfcollection. *Atmos. Res.*, **59–60**, 265–281, doi:10.1016/S0169-8095(01)00126-0.

——, A. Khain, U. Blahak, and K. D. Beheng, 2005: Possible effects of collisional breakup on mixed-phase deep convection simulated by a spectral bin cloud model. *J. Atmos. Sci.*, **62**, 1917–1931, doi:10.1175/JAS3432.1.

——, U. Blahak, and R. Buhr, 2014: On the analytic approximation of bulk collision rates of non-spherical hydrometeors. *Geosci. Model Dev.*, **7**, 463–478, doi:10.5194/gmd-7-463-2014.

Shima, S., K. Kusano, A. Kawano, T. Sugiyama, and S. Kawahara, 2009: The super-droplet method for the numerical simulation of clouds and precipitation: A particle-based and probabilistic microphysics model coupled with a non-hydrostatic model. *Quart. J. Roy. Meteor. Soc.*, **135**, 1307–1320, doi:10.1002/qj.441.

Stevens, B., 2007: On the growth of layers of nonprecipitating cumulus convection. *J. Atmos. Sci.*, **64**, 2916–2931, doi:10.1175/JAS3983.1.

——, and A. Seifert, 2008: Understanding macrophysical outcomes of microphysical choices in simulations of shallow cumulus convection. *J. Meteor. Soc. Japan*, **86A**, 143–162, doi:10.2151/jmsj.86A.143.

——, and Coauthors, 2005: Evaluation of large-eddy simulations via observations of nocturnal marine stratocumulus. *Mon. Wea. Rev.*, **133**, 1443–1462, doi:10.1175/MWR2930.1.

Ulbrich, C. W., 1983: Natural variations in the analytical form of the raindrop size distribution. *J. Climate Appl. Meteor.*, **22**, 1764–1775, doi:10.1175/1520-0450(1983)022<1764:NVITAF>2.0.CO;2.

van Zanten, M. C., and Coauthors, 2011: Controls on precipitation and cloudiness in simulations of trade-wind cumulus as observed during RICO. *J. Adv. Model. Earth Syst.*, **3**, M06001, doi:10.1029/2011MS000056.

Wacker, U., and A. Seifert, 2001: Evolution of rain water profiles resulting from pure sedimentation: Spectral vs. parameterized description. *Atmos. Res.*, **58**, 19–39, doi:10.1016/S0169-8095(01)00081-3.

——, and C. Lüpkes, 2009: On the selection of prognostic moments in parameterization schemes for drop sedimentation. *Tellus*, **61**, 498–511, doi:10.1111/j.1600-0870.2009.00405.x.

Walko, R. L., W. R. Cotton, M. P. Meyers, and J. Y. Harrington, 1995: New RAMS cloud microphysics parameterization. Part I: The single-moment scheme. *Atmos. Res.*, **38**, 29–62, doi:10.1016/0169-8095(94)00087-T.

Zhang, G., J. Vivekanandan, and E. A. Brandes, 2001: A method for estimating rain rate and drop size distribution from polarimetric radar measurements. *IEEE Trans. Geosci. Remote Sens.*, **39**, 830–841, doi:10.1109/36.917906.

——, ——, E. Brandes, R. Meneghini, and T. Kozu, 2003: The shape–slope relation in observed gamma raindrop size distributions: Statistical error or useful information? *J. Atmos. Oceanic Technol.*, **20**, 1106–1119, doi:10.1175/1520-0426(2003)020<1106:TSRIOG>2.0.CO;2.